MATLAB/Simulink Pulse-Echo Ultrasound System Simulator Based on Experimentally Validated Models

Taehoon Kim, Sangmin Shin, Hyongmin Lee, Hyunsook Lee, Heewon Kim, Eunhee Shin, and Suhwan Kim, *Senior Member, IEEE*

***Abstract*—A flexible clinical ultrasound system must operate with different transducers, which have characteristic impulse responses and widely varying impedances. The impulse response determines the shape of the high-voltage pulse that is transmitted and the specifications of the front-end electronics that receive the echo; the impedance determines the specification of the matching network through which the transducer is connected. System-level optimization of these subsystems requires accurate modeling of pulse-echo (two-way) response, which in turn demands a unified simulation of the ultrasonics and electronics. In this paper, this is realized by combining MATLAB/Simulink models of the high-voltage transmitter, the transmission interface, the acoustic subsystem which includes wave propagation and reflection, the receiving interface, and the front-end receiver. To demonstrate the effectiveness of our simulator, the models are experimentally validated by comparing the simulation results with the measured data from a commercial ultrasound system. This simulator could be used to quickly provide system-level feedback for an optimized tuning of electronic design parameters.**

***Index Terms*—Behavioral modeling, design optimization, impedance matching, MATLAB, ultrasonic imaging, ultrasonic transducers.**

I. Introduction

ULTRASOUND imaging has been applied to many clinical applications, including obstetrics, gynecology, orthopedics, emergency medicine, and the detection of cancer. Ultrasound imaging provides immediate data, facilitating speedy diagnosis and reducing cost. The type of transducer required varies across different applications, and transducers commonly have different impedance values and impulse responses. For example, an annular array transducer is required for steerable continuous-wave (CW) Doppler measurements of the heart, whereas an array with a tight convex curvature is required for imaging between the ribs [1].

The design of ultrasound systems capable of operating with a wide range of transducers poses several problems. One key challenge is the impedance mismatch which commonly occurs because the impedance of different transducers can vary from less than $50\,\Omega$ to $10\,\mathrm{k}\Omega$ [2], [3], while the impedance of the electronics is fixed. Mismatched impedances can seriously compromise the effectiveness of an ultrasound system, even if the transducer and electronics individually have outstanding performance. To maximize the efficiency with which the signal power is transferred requires a matching network, and a different network must be designed for each configuration.

Another challenge is that the electronics need to be designed appropriately for different types of transducers [3]. A transducer is driven by a high-voltage transmitter, which must generate a pulse with a shape that suits the impulse response of that transducer. The parameters of all the components in the front-end receiver, including the gains of amplifiers, the bandwidths of filters, and the sampling-rate and resolution of the analog-to-digital converter (ADC) will be determined by the transducer's two-way impulse response.

Despite these interdependencies, the transducers and the electronics in an ultrasound system are commonly developed independently, making it difficult to optimize performance. This motivates our development of a pulse-echo ultrasound system simulator. Most previous studies [4]–[14] have only focused on the modeling of the transducer and ultrasound field as an equivalent electrical circuit. The modeling of transducers themselves [4]–[9] has largely been based on theoretical models, such as those of Mason [10], Redwood [11], Krimholtz, Leedom and Matthaei (KLM) [12], and Leach [13]. These theoretical models, based on knowledge of the transducers' material properties and physical dimensions, are best suited to the optimization of a transducer during its design and manufacture.

Alternatively, an analytical model based on experimental measurements allows system designers to simulate transducers without reference to their physical specifications [14]. To combine a model of this sort with electronics within, an analog circuit simulator requires the transducer model to be transformed to a lumped passive-circuit model. Moreover, system-level simulation using an analog simulator requires a time-consuming transistor-level design of the electronics, and these circuits still have to be redesigned to permit a full analysis of subsequent parameter changes.

A third possibility, which allows a system designer to investigate the behavior of a pulse-echo ultrasound system from a more complete electro-acoustic point of view, is to simulate both the transducer and the electronics in the same high-level environment. In this paper, we present a simulator of this type, in which both the ultrasound components and the electronics of a pulse-echo ultrasound system are represented by a single MATLAB/Simulink model.

This approach supports a two-way (transmit and receive) analysis of ultrasound system. Unlike other simulators

Manuscript received September 22, 2015; accepted December 8, 2015. Date of publication December 11, 2015; date of current version January 26, 2016. This work was supported in part by the R&D Program of MOTIE/KEIT (10054578, Development of core technology for 9-axis smart motion sensor) and in part by Alpinion Medical Systems.

T. Kim, S. Shin, H. Lee, and S. Kim are with the Department of Electrical and Computer Engineering and the Inter-University Semiconductor Research Center (ISRC), Seoul National University, Seoul 151-744, South Korea (e-mail: suhwan@snu.ac.kr).

H. Lee, H. Kim, and E. Shin are with Alpinion Medical Systems, Seoul 152-848, South Korea.

Digital Object Identifier 10.1109/TUFFC.2015.2508148

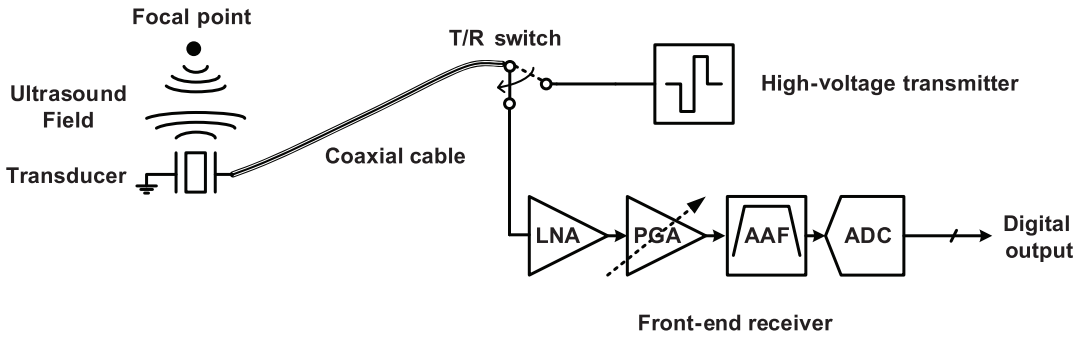

Fig. 1. Block diagram of a pulse-echo ultrasound system.

[15]–[19], high-voltage pulse generation, electrical signal conditioning, and analog-to-digital conversion can be simulated with the transducer. Modeling the transducer as a transfer function, which can be derived from pulse-echo measurements made during manufacturing, makes it easy to change the transducer in the simulation. Moreover, by inserting transfer functions into the signal path to account for the impedances of both the transducer and the electronics, impedance mismatches can be analyzed and corrected.

Our simulator includes all the parameters that the designers of an ultrasound system require to specify the electronics. Thus, the best pulse for a given transducer can be determined using the high-voltage transmitter model and, since the front-end receiver model is based on a specific architecture, the specifications of each component in the receiver can readily be determined. Finite-element modeling (FEM) can also be considered to simulate the electronics. It is also a powerful tool but with complicated and time-consuming method [20]. On the other hand, our approach reduces the simulation time while keeping high accuracy and it is able to provide the microelectronics designers with affordable system-level feedback in a short time [21].

We verified the accuracy of our simulator, by starting with preliminary tests on individual subsystem models. Then, experiments on the complete system were conducted using a commercial ultrasound system connected to the transducer. Our simulation of the most important signals, which are the electrical pulse from the high-voltage transmitter, the echo signal from the acoustic subsystem, and the digitized output of the front-end receiver, showed good agreement with experimental results.

This paper is organized as follows. In Section II, we introduce the architecture of a pulse-echo ultrasound system. In Section III, the building blocks of the proposed simulator are presented and the MATLAB/Simulink implementation of the subsystems is described in detail. In Section IV, we present the results of experiments designed to validate the accuracy of our simulator. We draw conclusions in Section V.

II. Overview of a Pulse-Echo Ultrasound System and Our Simulation

Fig. 1 shows the block diagram of a pulse-echo ultrasound system, consisting of a high-voltage transmitter, a transducer, an ultrasound field, a coaxial cable, and a front-end receiver. In transmit mode, an electrical pulse is generated by the high-voltage transmitter, causing the transducer to produce an acoustic pulse which propagates toward a focal point, reflecting off any object in its path. In receive mode, the transducer picks up the returning acoustic echo, which is converted into an electrical echo signal and processed by the front-end receiver.

The front-end receiver contains a transmit/receive (T/R) switch, which blocks the high-voltage pulses during the reception; a low-noise amplifier (LNA), which acts as a preamplifier; a programmable-gain amplifier (PGA), which provides time-gain compensation to allow for the way in which the returning echo signal is attenuated by body tissues as a function of the distance traveled; an antialiasing filter (AAF), which restricts the bandwidth of the signal to satisfy the Nyquist-Shannon sampling theorem over the band of interest; and an ADC, which digitizes the electrical echo signal for subsequent image processing [22].

The block diagram in Fig. 2 shows the main units of the proposed simulator. A system designer can configure the parameters of the high-voltage transmitter model to generate desired particular high-voltage pulse in transmit mode. The front-end receiver model simulates electrical signal conditioning and analog-to-digital conversion in receive mode, taking into account the most significant nonidealities, such as sampling clock jitter, noise, and harmonic distortion.

The acoustic subsystem that we model consists of a coaxial cable, a transducer, and an ultrasound field. The acoustic subsystem model is based on the electroacoustic transfer function *H(s)*, which represents the acoustic process which transforms an outgoing electrical pulse $V_{\rm t}(t)$ into an incoming electrical echo signal $V_{\rm r}(t)$. This process involves electro-acoustic conversion of the transmitted pulse, acoustic propagation, reflection, and acoustic-electrical conversion of the echo signal. *H(s)* can be expressed as the ratio between $V_{\rm t}(s)$ and $V_{\rm r}(s)$, which are, respectively, the Laplace transforms of $V_{\rm t}(t)$ and $V_{\rm r}(t)$.

To simulate the voltage division by the impedances of the subsystems, models of the interfacing electronics are inserted between the models of two subsystems. In transmit mode, a model of the transmitter (TX) interfacing electronics acting as a voltage divider based on transfer function $Z_{\rm TX}(S)$ is inserted between the high-voltage transmitter model and the acoustic subsystem model. The impedance Z_a of the acoustic subsystem is the load impedance, as seen by the high-voltage transmitter, and the output impedance Z_t of the high-voltage transmitter is the source impedance. Thus, the amplitude of an electrical pulse $V_{\rm TX}(t)$ from the high-voltage transmitter needs to be multiplied

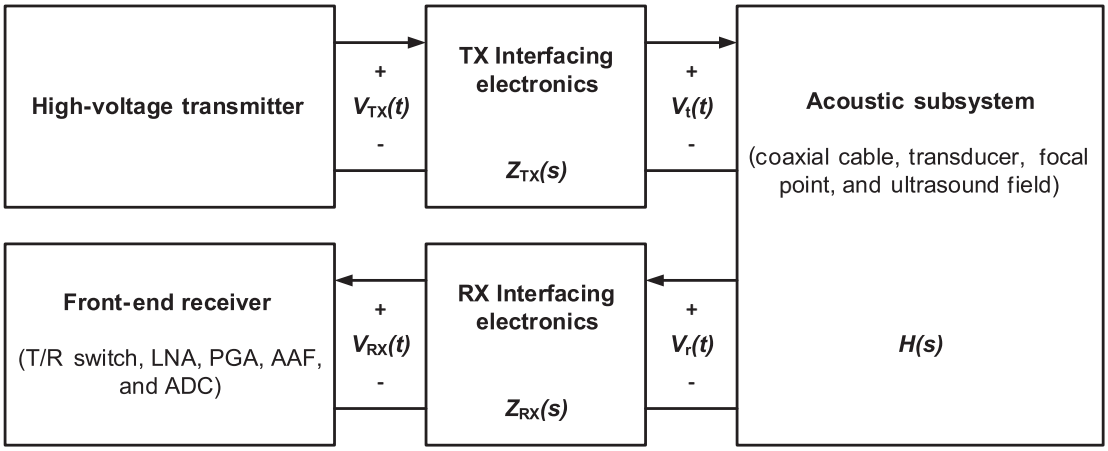

Fig. 2. Model of the pulse-echo ultrasound system shown in Fig. 1, consisting of five subsystem models. The electronic components in the system are simulated in the high-voltage transmitter model and the front-end receiver model. The acoustic behavior of the ultrasound field and the effect of coaxial cable are modeled as the acoustic subsystem, based on the electroacoustic transfer function *H(S)*. To express division of the voltage by the impedances of the subsystems, the transfer functions $Z_{\mathrm{TX}}(S)$ and $Z_{\mathrm{RX}}(S)$, representing the interfacing electronics, are inserted between the models of the electronics and the acoustic subsystem.

by $Z_a/(Z_t + Z_a)$, if it is to correspond to the electrical pulse $V_t(t)$ that reaches the acoustic subsystem.

In receive mode, a model of the receiver (RX) interfacing electronics based on the transfer function $Z_{\mathrm{RX}}(S)$ is inserted between the acoustic subsystem model and the front-end receiver model. The impedance Z_a of the acoustic subsystem is the source impedance and the input impedance Z_r of the front-end receiver is the load impedance as seen by the acoustic subsystem connected to the front-end receiver. Thus, the amplitude of the electrical echo signal $V_r(t)$ acquired by the transducer needs to be multiplied by $Z_r/(Z_a + Z_r)$, if it is to correspond to the electrical echo signal $V_{\mathrm{RX}}(t)$ that is sent to the front-end receiver.

III. Modeling Subsystems

A. High-Voltage Transmitter Model

Most ultrasound transmitters can be classified as pulse-type or burst-type. Theoretically, an ideal pulse-type transmitter generates a single spike, which is the waveform that produces the best axial resolution. However, a real transducer has a bandpass response, and the pulse that is actually generated needs to be appropriate for the response of that particular transducer. A burst-type transmitter generates several cycles of a square wave or a sinusoid, modulated by a window (such as a Hamming window). Since the amount of energy that can be transmitted into a patient's body is limited by medical authorities, the voltage generated by the transmitter needs to be lower when the pulse train is longer.

Fig. 3 shows our model, in which the high-voltage transmitter is simulated by relatively simple blocks; nevertheless, the amplitude of the pulse, offset, period, and duty cycles are controllable, and multiple square or sine waves can easily be generated. The best pulse for a particular application can be determined by examining the simulated returning echo signal for different transmitted pulse. Additionally, the multiport switch block allows the simulated output of the high-voltage transmitter to be replaced by measured data.

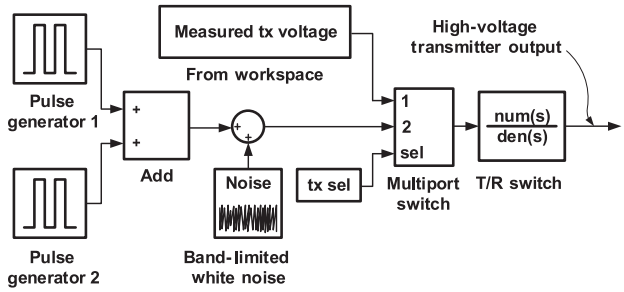

Fig. 3. Simulink model of the high-voltage transmitter.

B. Acoustic Subsystem Model and Interfacing Electronics Model

From the description in Section II, the complete transfer function from the transmitted pulse $V_{\mathrm{TX}}(t)$ to the received echo signal $V_{\mathrm{RX}}(t)$ can be written as follows:

$$\frac{V_{\mathrm{RX}}(s)}{V_{\mathrm{TX}}(s)} = Z_{\mathrm{TX}}(s)H(s)Z_{\mathrm{RX}}(s) = \frac{Z_{\mathrm{a}}}{Z_{\mathrm{t}} + Z_{\mathrm{a}}}(s)H(s)\frac{Z_{\mathrm{r}}}{Z_{\mathrm{a}} + Z_{\mathrm{r}}}(s) \quad (1)$$

where $V_{\mathrm{TX}}(s)$ and $V_{\mathrm{RX}}(s)$ are, respectively, the Laplace transforms of $V_{\mathrm{TX}}(t)$ and $V_{\mathrm{RX}}(t)$. In order to model this transfer function using MATLAB/Simulink, we have measured the output impedance $Z_t(j2\pi f_k)$ of the high-voltage transmitter and the input impedance $Z_r(j2\pi f_k)$ of the front-end receiver at 949 frequencies ranging from 1 to 20 MHz. To obtain the measured data, Agilent HP4194A impedance analyzer and ECUBE7 ultrasound system are connected by calibrated impedance probe. We have also measured the impedance $Z_a(j2\pi f_k)$ of the transducer with the 2.3-m coaxial cable. The L3–12 transducer that has 128-elements and 8.5-MHz center frequency is used in this measurement. Both ECUBE7 ultrasound system and L3–12 transducer are the commercial product developed from Alpinion Medical Systems. Values of the vectors $\boldsymbol{Z}_a(j2\pi f_k)/(\boldsymbol{Z}_t(j2\pi f_k) + \boldsymbol{Z}_a(j2\pi f_k))$

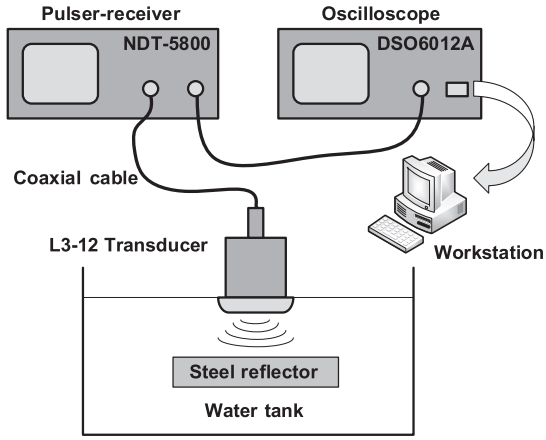

Fig. 4. Setup for the pulse-echo measurements required to build the electroacoustic transfer function *H(s)*.

and $\boldsymbol{Z}_r(j2\pi f_k)/(\boldsymbol{Z}_a(j2\pi f_k) + \boldsymbol{Z}_r(j2\pi f_k))$ in the complex plane were obtained from the measured data. The transfer functions $Z_{\mathrm{TX}}(S)$ and $Z_{\mathrm{RX}}(S)$ were then computed using the *rationalfit* function in MATLAB to fit a function of the following form to the complex vector data [23], [24]:

$$F(s) = \sum_{k=1}^{N} \frac{\text{residue}_k}{s\text{-pole}_k} \tag{2}$$

where *N* is the number of poles.

We also need to measure $V_t(j2\pi f_k)$ and $V_r(j2\pi f_k)$ in the frequency domain, in order to build the transfer function *H*(*s*). We made pulse-echo measurements using the setup shown in Fig. 4. A Panametrics NDT-5800 pulser–receiver sends a high-voltage pulse to the transducer, which sends an acoustic wave toward a steel reflector in a water tank, and awaits echoes. The echoes received by the pulser–receiver are measured using an Agilent DSO6012A oscilloscope, which samples the echo signal every 5 ns, and transfers the digitized sample to a workstation. Measurements of $V_t(t_k)$ and $V_r(t_k)$ at sampling time t_k are converted, respectively, into $V_t(j2\pi f_k)$ and $V_r(j2\pi f_k)$, in the frequency domain, by discrete Fourier transform. $V_t(j2\pi f_k)$ is the product of $V_{\mathrm{TX}}(j2\pi f_k)$ and $Z_{\mathrm{a}}(j2\pi f_k)/(Z_{\mathrm{t}}(j2\pi f_k) + Z_{\mathrm{a}}(j2\pi f_k))$. From this frequency domain data, we can find $H(j2\pi f_k)$ from the ratio $V_r(j2\pi f_k)/V_t(j2\pi f_k)$. We can then compute *H*(*s*) by calling the *rationalfit* function, as we did to obtain $Z_{\mathrm{TX}}(S)$ and $Z_{\mathrm{RX}}(S)$. The transducer has its own axial intensity profile, so the magnitude of the transfer function *H*(*s*) changes depending on the distance between the transducer and the reflector. However, the transducer's significant properties in the system-level optimization, such as center frequency, bandwidth, and impedance, are not affected by the distance. Therefore, the overall direction of system development does not change. In our experiment, we have measured transducer properties with 20-mm distance that is focal depth of the transducer. Although the distance between transducer and steel reflector can slightly affect transfer function *H*(*s*) with the attenuation of medium, we assume that the attenuation coefficient of water (0.0022 dB/MHz/cm) is small enough to be neglected for our study.

The Simulink models of the TX interfacing electronics, the acoustic subsystem, and the RX interfacing electronics consist of a number of transfer function blocks, together with an add block. The poles and relevant residues of a transfer function can be converted, respectively, to the numerator and denominator of a transfer function block in the Simulink environment, as shown in Fig. 5. $Z_{\mathrm{TX}}(S)$, *H*(*s*), and $Z_{\mathrm{RX}}(S)$ has 77, 300, and 19 poles, respectively. To ensure that every transfer function block has real coefficients, each block represents either one real pole, or a pair of complex conjugate poles. Consequently, each Simulink model of the TX interfacing electronics, acoustic subsystem, and RX interfacing electronics has 39, 151, and 11 transfer function blocks.

C. Front-End Receiver Model

Our Simulink model of a front-end receiver, shown in Fig. 6, consists of a transfer function block, the T/R switch, and eight subsystem blocks, which model: harmonic distortion, the LNA, the voltage-controlled attenuator (VCAT), the PGA, the high-pass filter (HPF), the low-pass filter (LPF), sampling clock jitter, and the ADC.

Fig. 7 shows an equivalent circuit model of the T/R switch [25]. The values of R_s, R_p, and C_p are 13 Ω, 100 kΩ, and 40 pF, respectively. R_{IN} and C_{IN} are the input resistance and the input capacitance of the LNA. R_F is a shunt feedback resistor for an active input termination, which is preferred in ultrasound applications because it reduces the reflections resulting from mismatches and achieves better axial resolution without a significant increase in noise. The input impedance $Z_{\mathrm{IN,ActiveTermination}}$ of the LNA under the active termination approximately follows:

$$Z_{\text{IN, Acitve Termination}} = \frac{R_{\mathrm{F}}}{1 + \frac{A_{\mathrm{V,LNA}}}{2}} \tag{3}$$

where $A_{\mathrm{V,LNA}}$ is the voltage gain of the LNA. The equivalent input impedance of the LNA can be expressed as follows [26]:

$$\begin{aligned} Z_{\mathrm{IN}}(s) &= Z_{\text{IN, Active Termination}} \| R_{\mathrm{IN}} \| C_{\mathrm{IN}} \\ &= \frac{R_{\mathrm{IN}} R_{\mathrm{F}}}{R_{\mathrm{F}} R_{\mathrm{IN}} C_{\mathrm{IN}} s + \left(1 + \frac{A_{\mathrm{V,LNA}}}{2}\right) R_{\mathrm{IN}} + R_{\mathrm{F}}}. \end{aligned} \tag{4}$$

Without active termination, the value of the feedback resistor R_F is effectively infinite. The transfer function of the T/R switch under the active termination configuration can be expressed as follows:

$$\frac{V_{\text{T/R switch output}}}{V_{\text{front-end receiver input}}}(s) = \frac{2R_p}{R_s R_p C_p s + R_s + 2R_p} \cdot \frac{2Z_{\mathrm{IN}}(s)}{R_s + 2Z_{\mathrm{IN}}(s)}. \tag{5}$$

The transfer function block which models the T/R switch is shown at the top left in Fig. 6.

Fig. 8 is a detailed block diagram which explains how the subsystems of the front-end receiver are modeled. Fig. 8(a) shows the model of harmonic distortion. The model is placed between T/R switch and the LNA to express the signal

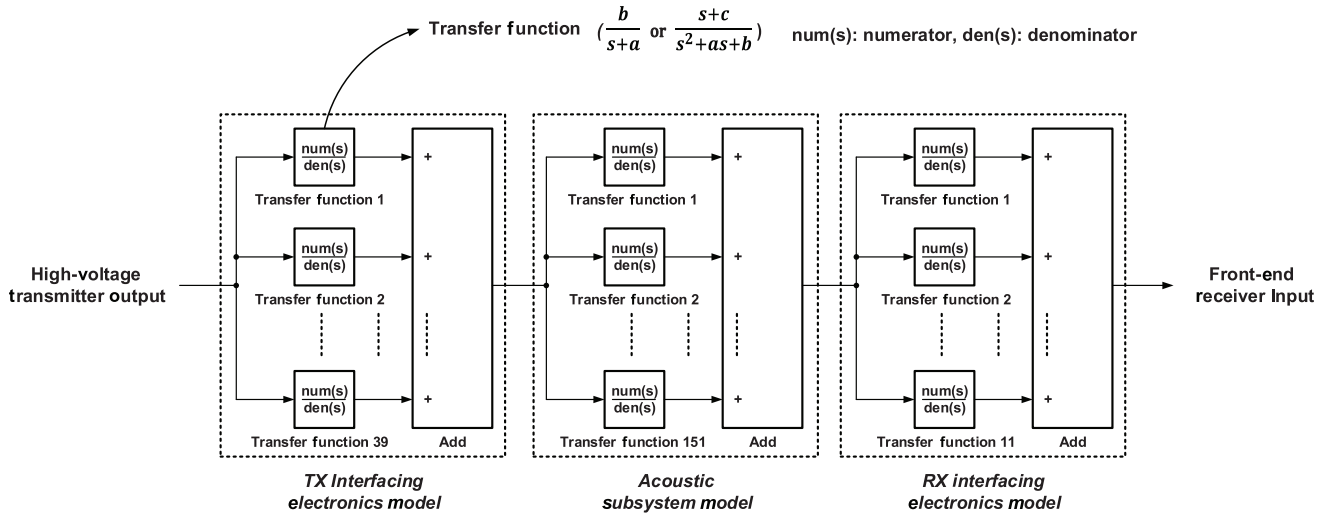

Fig. 5. Simulink models of the TX interfacing electronics, acoustic subsystem, and RX interfacing electronics based, respectively, on the transfer functions $Z_{\mathrm{TX}}(S)$, *H(s)*, and $Z_{\mathrm{RX}}(S)$.

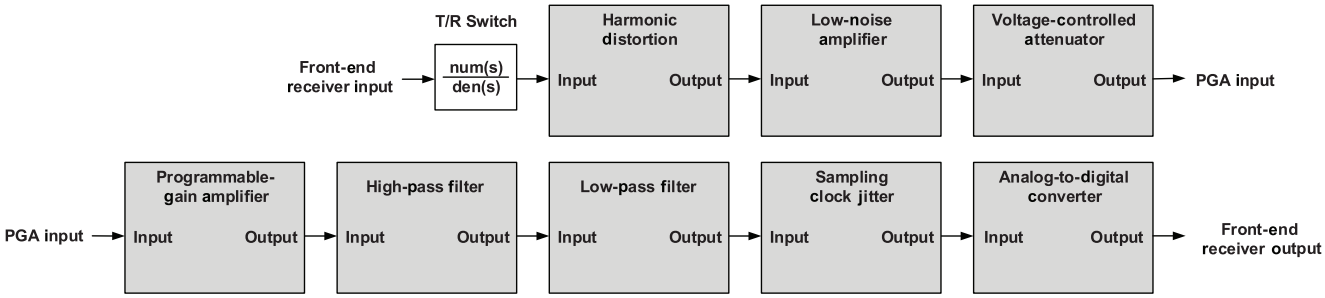

Fig. 6. Simulink model of the front-end receiver.

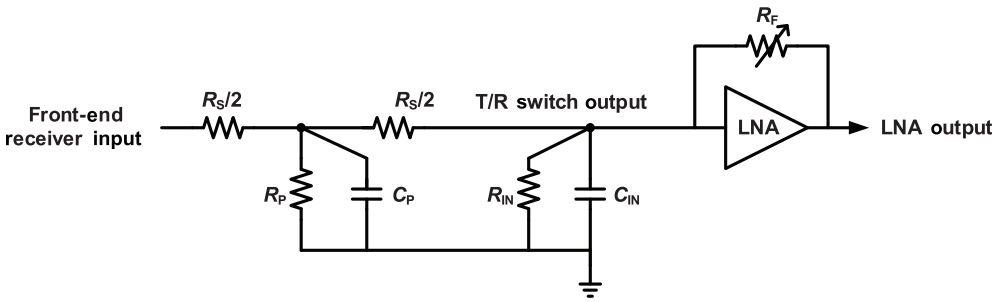

Fig. 7. Equivalent circuit model of the T/R switch under considering the active input termination.

distortion introduced by the nonlinearities of the amplifiers and ADC in the front-end receiver. The harmonic distortion is not shown in Fig. 7, because it is not a specific circuit but a phenomenon from following circuits.

The parameter value of the constant block controls the order of the harmonic distortion, and the gain changes its power. Fig. 8(b) shows the model of the amplifier used in the LNA, VCAT, and PGA subsystem blocks. The gain and transfer function model the amplifier's finite gain and bandwidth. The rate limiter models the amplifier's slew-rate, and the saturation block models the output swing. Our Simulink model of the front-end receiver also includes a model of amplifier noise, which is a crucial difference between a real and an ideal circuit. This amplifier noise is made up of current and voltage noise, together with thermal noise from the source resistance. Several noise-modeling blocks have been introduced into the LNA, VCAT, and PGA subsystem blocks to simulate the band-limited white noise of the input voltage, current noise from the LNA, and the input voltage noise from the PGA and VCAT. The total voltage-noise density of the output of the amplifier can be expressed as follows:

$$E_{\mathrm{O}} = \sqrt{e_N^2 + (i_N R_{\mathrm{source}})^2 + 4K_B T R_{\mathrm{source}}} \qquad (6)$$

where e_N is the voltage noise density of the amplifier. The term $i_N R_{\mathrm{source}}$ is the product of the voltage contribution of current-noise density and the source resistance, which has a thermal-noise density of $(4K_B T R_{\mathrm{source}})^{1/2}$. The source

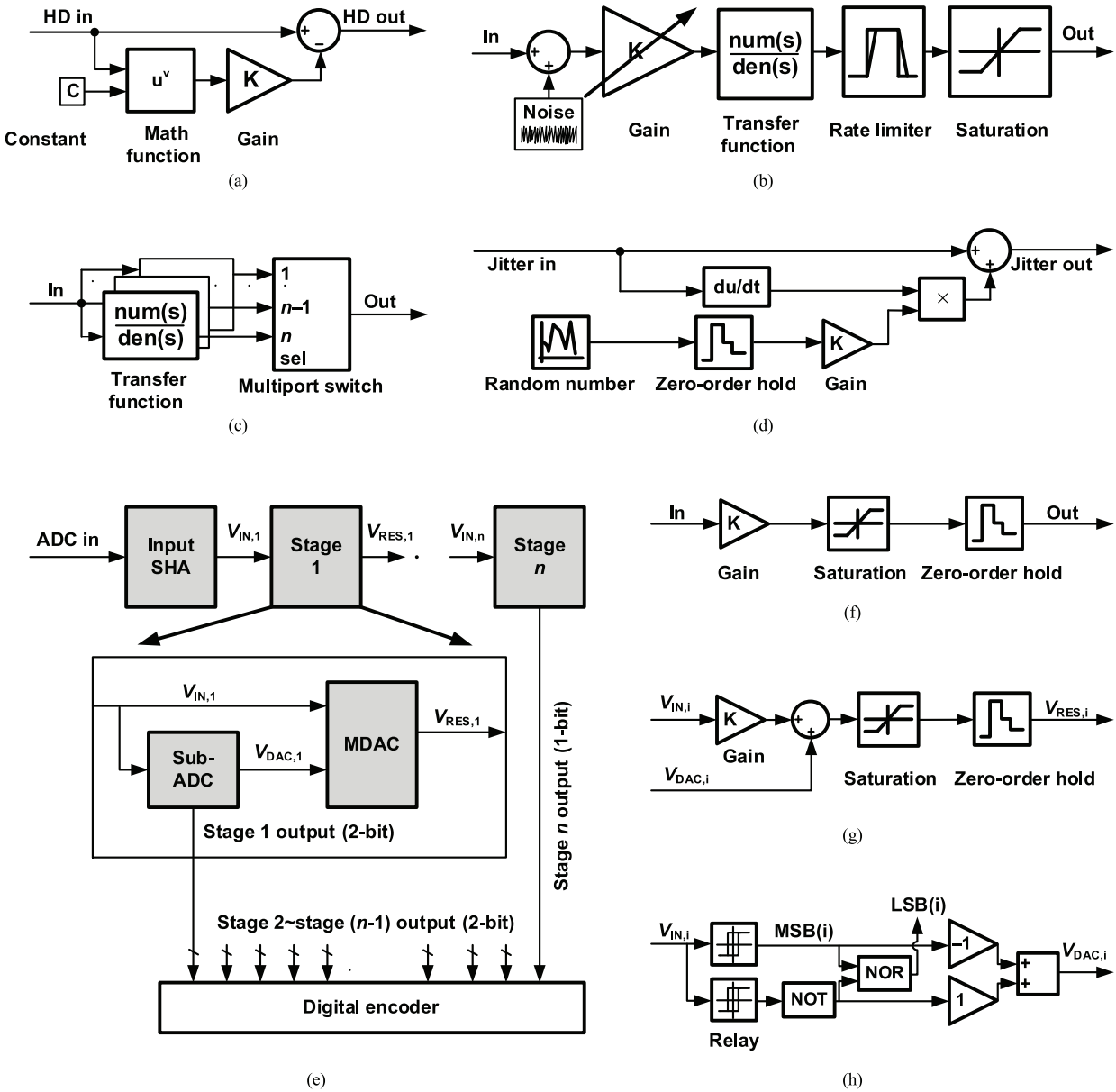

Fig. 8. Block diagram of our Simulink model of the front-end receiver: (a) harmonic distortion, (b) LNA, VCAT, and PGA with variable gain, (c) HPF and LPF with selective bandwidth, (d) sampling clock jitter, (e) ADC, (f) input SHA in ADC, (g) MDAC in *i*th stage, and (h) sub-ADC in *i*th stage.

resistance R_{source} is the impedance of the transducer, and is therefore likely to vary widely with the type of transducer in use. Fig. 8(c) shows the HPF and LPF subsystems, in each of which the filter is represented by a transfer function, and this can be changed using the multiport switch to vary the bandwidth of the corresponding filter. Fig. 8(d) shows the model of sampling clock jitter, defined as a random variation of the sampling instant; the resulting noise is assumed to be uniformly distributed. The error introduced by a sinusoidal signal *x(t)* with amplitude *A* and frequency f_{in} can be calculated as in terms of the jitter deviation δ as follows [27]:

$$x(t+\delta) - x(t) \approx 2\pi f_{\text{in}} \delta A \cos(2\pi f_{\text{in}} t) = \delta \frac{dx(t)}{dt} \quad (7)$$

and this equation is the basis of our jitter model. The ADC in an ultrasound system requires a sampling-rate which is at least 40 MS/s, and a resolution between 10 and 14 bits. A pipelined ADC architecture is known to be able to satisfy these requirements, and that is what we have modeled as shown in Fig. 8(e). This ADC includes a sample-and-hold amplifier (SHA), several stages, and an encoder for digital correction, and each stage has a multiplying DAC (MDAC) and a sub-ADC. Fig. 8(f)–(h), respectively, shows the block diagrams of the SHA, the MDAC, and the sub-ADC, which is inside the ADC. The digital encoder is described using a MATLAB script.

IV. Experiments Versus Simulation

A. Validation of Subsystem Models

Before simulating the complete ultrasound system, we assessed the accuracy of each subsystem model. We started with the models of the acoustic subsystem and the interfacing

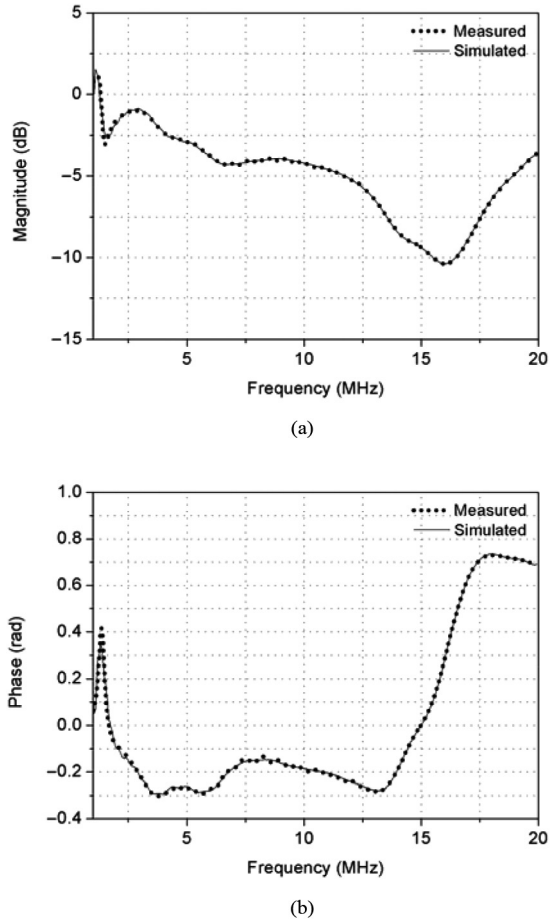

Fig. 9. Comparison between the transfer function $Z_{\mathrm{TX}}(S)$ and the experimental data $Z_{\mathrm{TX}}(j2\pi f_{\mathrm{k}})$, (a) magnitude and (b) phase, both against the frequency f_{k}.

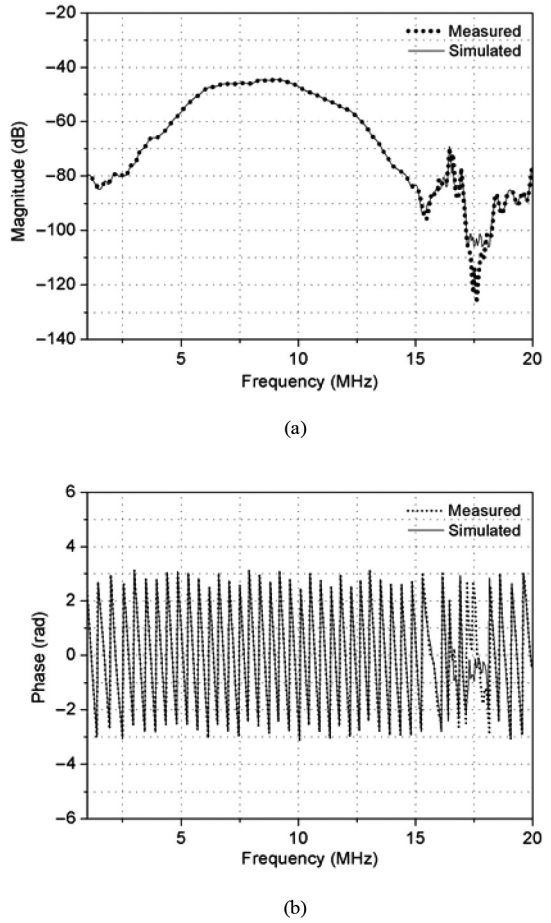

Fig. 10. Comparison between the transfer function *H(s)* and the experimental data $H(j2\pi f_{\mathrm{k}})$, (a) magnitude and (b) phase, both against the frequency f_{k}.

electronics, and investigated the accuracy of the approximate transfer functions $Z_{\mathrm{TX}}(S)$, *H*(*s*), and $Z_{\mathrm{RX}}(S)$ in the same context as shown in [14]. Fig. 9 compares the approximate transfer function $Z_{\mathrm{TX}}(S)$ obtained by calling the *rationalfit* function with the complex vector data $\boldsymbol{Z}_a(j2\pi f_k)/(\boldsymbol{Z}_t(j2\pi f_k) + \boldsymbol{Z}_a(j2\pi f_k))$, measured using an Agilent HP4194A impedance analyzer at 949 frequencies in the frequency domain. The difference between the curves can be expressed as follows:

$$10^{\varepsilon/20} \geq \frac{\sqrt{\sum_{k=1}^{n} |F_0\{f_k\} - F(s)|^2}}{\sqrt{\sum_{k=1}^{n} |F_0\{f_k\}|^2}} \tag{8}$$

where ε is the error in dB, F_0 is the measured value of $F_0(j2\pi f_{\mathrm{k}})$ at a frequency f_{k}, and $F(s = j2\pi f)$ is the approximation of the transfer function computed using the *rationalfit* function. On this basis, the error in $Z_{\mathrm{TX}}(S)$ is $-32.18\,\mathrm{dB}$. Fig. 10 shows similar results for *H*(*s*), and here the error is $-43.83\,\mathrm{dB}$. At around 17.5 MHz, there is a mismatch between the simulated and the measured signals, but this frequency is sufficiently distant from the carrier frequency that it contains no meaningful information. Fig. 11 shows further results for the transfer function $Z_{\mathrm{RX}}(s)$, and in this case the error is less than $-44\,\mathrm{dB}$.

We then turned to the model of the front-end receiver. We sent a sine wave with an amplitude of $8\,\mathrm{mV_{PP}}$ and frequency of 5 MHz to both the MATLAB/Simulink model and the front-end receiver in the ECUBE7 ultrasound system. The parameters of the front-end receiver, obtained from its datasheet [26], are summarized in Table I. The ability of our entire simulation, to predict system performance and image quality, depends on accurate modeling of the noise characteristics of the front-end receiver [3]. We can see from (6) that the controllable parameters related to the noise of the front-end receiver include the source impedance, and the gain of the LNA and PGA. The source impedance contributes to the second and third terms in (6), which are the densities of input current noise and thermal noise. The gain of the LNA and PGA affect the first term of (6) which is the input voltage noise density [26]. We compared the narrowband signal-to-noise ratio (NBSNR) of the simulated and measured results for different combinations of LNA and PGA gain, and different source impedances. The source impedance of the front-end receiver was changed by inserting termination resistors with values of 50, 120, and $240\,\Omega$ between the input of the front-end receiver and ground. We also compared the spurious-free dynamic range (SFDR) of the simulated and measured results to assess the accuracy with which distortion is modeled. Tables II and III compare measured values of NBSNR and SFDR with simulation results.

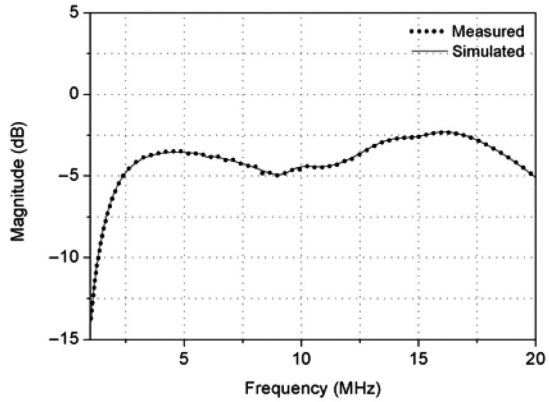

(a)

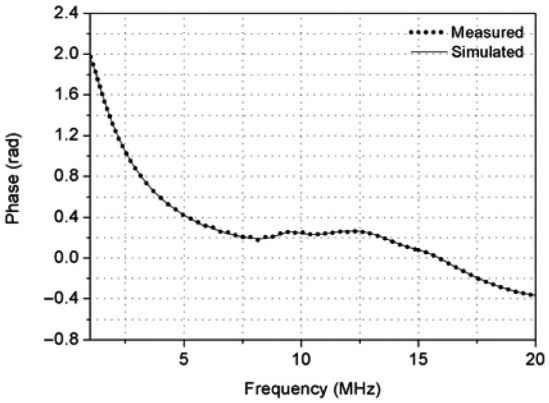

(b)

Fig. 11. Comparison between the transfer function $Z_{\mathrm{RX}}(S)$ and the experimental data $Z_{\mathrm{RX}}(j2\pi fk)$, (a) magnitude and (b) phase, both against the frequency f_{k}.

TABLE I
FRONT-END RECEIVER PARAMETERS IN THE MATLAB/SIMULINK MODEL

Parameter	Value	Units
Low-noise amplifier (LNA)		
Input resistance	8	kΩ
Input capacitance	20	pF
Gain	12, 18, 24	dB
Bandwidth	70	MHz
Input voltage noise over gain	0.9, 0.7, 0.63	nV/√Hz
Input current noise	2.7	pA/√Hz
Voltage controlled attenuator (VCAT)		
Attenuation	0 to –40 (9 steps)	dB
Input voltage noise over attenuation	2 to 10.5 (9 steps)	nV/√Hz
Programmable gain amplifier (PGA)		
Gain	24, 30	dB
Bandwidth	70	MHz
Input voltage noise	1.75	nV/√Hz
Full-scale range	3.3	V
Antialiasing filter (AAF)		
Low cut-off frequency	50, 100, 150	kHz
High cut-off frequency	10, 15, 20, 30	MHz
Analog-to-digital converter		
Sampling clock jitter	20	ps
Input range	2	V
Sampling-rate	40, 65	MS/S
Resolution	12, 14	bits

We assessed our model of the high-voltage transmitter as part of our validation of the complete system by comparing the simulated output waveform of the model to measured high-voltage pulses while inputting the same parameters to the signal generator block in the model and the high-voltage transmitter in the ECUBE7 ultrasound system.

B. Validation of the Complete System Model

After they had been checked individually, the subsystem models were integrated in to a system model. We then carried out experiments on the complete system to verify correct pulse-echo operation. The experimental setup is shown in Fig. 12. The L3–12 transducer immersed in a water tank is connected by a coaxial cable to an ECUBE7 ultrasound system. The transducer is excited by pulses from the high-voltage transmitter in the ECUBE7, and produces the ultrasonic waves which propagate through the water and are reflected by a steel reflector. By exciting the transducer with a low-voltage signal (tens of volts), it is possible to avoid the nonlinearity of the water [28]. The same transducer converts the returning sound to an electrical echo signal. The transmitted high-voltage pulse and received echo signal can be visualized on an oscilloscope. The electrical echo signal goes through amplification, filtering, and analog-to-digital conversion by the front-end receiver in the ECUBE7.

Fig. 13 shows block diagrams of the experimental setup with the pulse-echo ultrasound system operating in transmit and receive modes. $V(1)$ is the electrical pulse from the high-voltage transmitter, $V(2)$ is the electrical echo signal from the acoustic subsystem, and $V(3)$ is the digital output of the front-end receiver. The high-voltage pulse $V(1)$ and the echo signal $V(2)$ were sampled every 5 ns, and the digital output of the echo signal $V(3)$ was acquired every 25 ns. Agilent 10076C high-voltage probe, which supports maximum 4-kV input voltage, was used to measure the high-voltage pulse $V(1)$.

We will now compare the signals obtained from experiments and simulations. Fig. 14 compares the measured waveform of the high-voltage pulse $V(1)$ in Fig. 13 with the simulated waveform from the high-voltage transmitter model. The amplitudes of these signals are normalized, so the received echo signal has a peak amplitude of unity. We are able to input either the measured or the simulated version of this waveform to the acoustic subsystem in our simulation; however, we found that this produces no appreciable difference to the received echo signal, suggesting that the waveforms are very similar indeed.

Fig. 15 compares the waveform of the received echo signal $V(2)$ in Fig. 13, measured between the acoustic subsystem and

TABLE II
MEASURED AND SIMULATED VALUES OF NBSNR OF THE FRONT-END RECEIVER FOR DIFFERENT COMBINATIONS OF LNA AND PGA GAIN, AND WITH DIFFERENT TERMINATION RESISTORS

Termination resistor (Ω)	LNA gain (dB)	PGA gain (dB)	Measured NBSNR* (dB)	Simulated NBSNR* (dB)	Error (dB)
50	12	24	39.68	39.42	0.26
		30	38.68	39.42	–0.74
	18	24	40.48	40.82	–0.34
		30	40.41	40.86	–0.45
	24	24	40.99	41.5	–0.51
		30	42.05	41.52	0.53
120	12	24	45.82	44.66	1.16
		30	44.61	45.06	–0.45
	18	24	45.52	46.07	–0.55
		30	45.55	46.08	–0.53
	24	24	45.83	46.65	–0.82
		30	50.14	46.68	3.46
240	12	24	48.68	48.16	0.52
		30	48.06	48.26	–0.2
	18	24	50	49.1	0.9
		30	49.07	49.15	–0.08
	24	24	48.18	49.52	–1.34
		30	50.14	49.58	0.56

*NBSNR (dB) $= 10 \times \log_{10}$ [signal power (V_{rms}^2)/sum of noise power in 2-MHz band around signal frequency (V_{rms}^2)].

TABLE III
MEASURED AND SIMULATED VALUES OF SFDR OF THE FRONT-END RECEIVER FOR DIFFERENT COMBINATIONS OF LNA AND PGA GAIN, AND WITH DIFFERENT TERMINATION RESISTORS

Termination resistor (Ω)	LNA gain (dB)	PGA gain (dB)	Measured SFDR* (dB)	Simulated SFDR* (dB)	Error (dB)
50	12	24	41.54	48.52	–6.98
		30	43.7	48.03	–4.33
	18	24	43.51	49.79	–6.28
		30	45.25	49.77	–4.52
	24	24	49.08	50.87	–1.79
		30	49.74	50.55	–0.81
120	12	24	51.3	54	–2.7
		30	54.95	54.52	0.43
	18	24	51.48	55.5	–4.02
		30	52.05	55.11	–3.06
	24	24	51.28	55.85	–4.57
		30	55.32	55.65	–0.33
240	12	24	55.94	54.42	1.52
		30	55.51	54.66	0.85
	18	24	55.82	54.1	1.72
		30	58.05	54.34	3.71
	24	24	50.11	54.21	–4.1
		30	55.97	54.3	1.67

*SFDR (dB) $= 10 \times \log_{10}$ [signal power (V_{rms}^2)/worst spurious signal power (V_{rms}^2)].

the front-end receiver, with the simulated waveform from the acoustic subsystem model. In Fig. 15(a), there is a noticeable divergence around 46.4 μs; otherwise, the curves show satisfactory agreement. Fig. 16 shows the digitized output $V(3)$ in Fig. 13 from the front-end receiver at a sampling rate of 40 MSPS.

Overall, these results suggest that our system model simulates the system-level behavior of a pulse-echo ultrasound system with sufficient fidelity to give it a place in the design process.

C. Discussion

One immediate application of our model is the design of a matching network, which can be implemented as a parallel compensating inductance, a series compensating inductance,

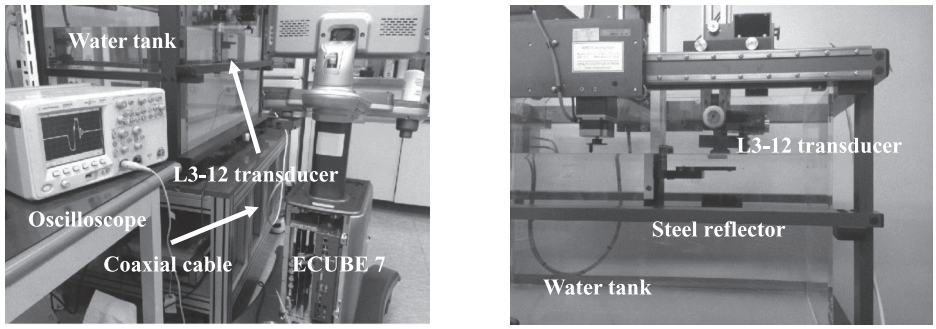

(a) (b)

Fig. 12. Photographs of (a) our experimental setup with (b) water tank.

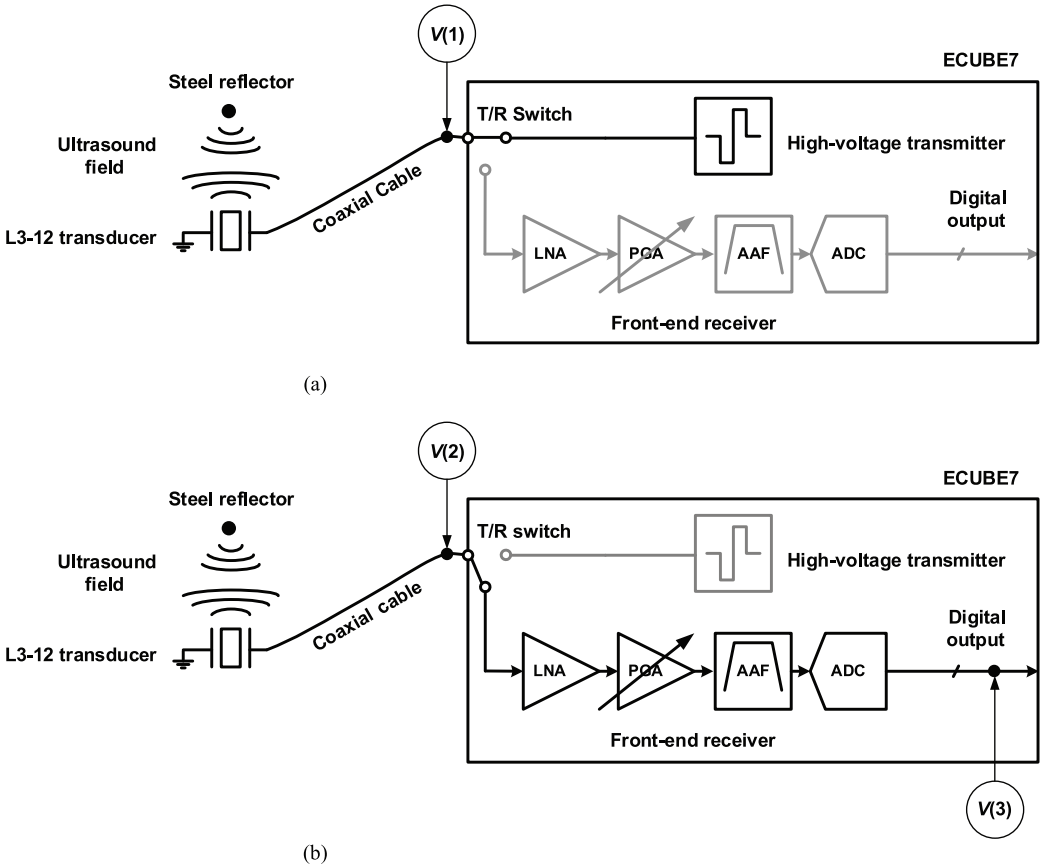

Fig. 13. Block diagram of a pulse-echo ultrasound system in (a) transmit and (b) receive mode.

or an L matching network [29]. For example, if we use a series compensating inductance, then we need to change the imaginary part of the transducer impedance Z_a. We can do this by adding a term $2\pi f_k L$ to the measured transducer impedance Z_a, recomputing the transfer functions $Z_{\mathrm{TX}}(S)$ and $Z_{\mathrm{RX}}(S)$, and rebuilding the Simulink model of the interfacing electronics.

We would expect to achieve more accurate matching than existing simulators, which model the ultrasound field but not the electronics. In particular, it is unsatisfactory to ignore the impedances of the high-voltage transmitter and the front-end receiver, and thus, selected values of the inductors may be far from optimal in the context of the whole system. This means that the matching network has to be redesigned for each transducer, and tested at the imaging level. Our simulator should reduce the need for these activities.

Our simulation can also help in choosing a good shape for the electrical pulse generated by the high-voltage transmitter, because a designer can observe the simulated echo signal as the shape of the transmitted pulse is changed. A designer can also search for system parameters which improve the final SNR, because the simulation includes the analog processes of amplification, filtering, and A/D conversion which take place in the front-end receiver. We can determine the most appropriate components in the front-end receiver by considering application requirements: the maximum gain required from the amplifiers

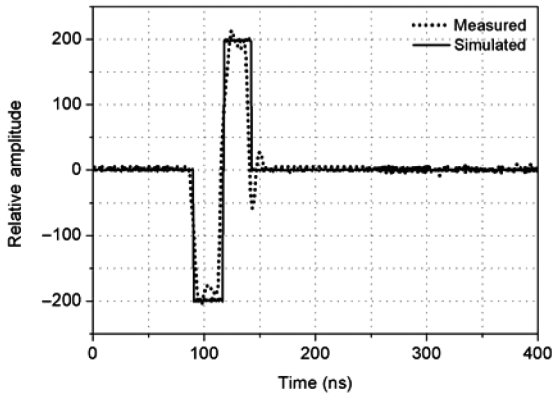

Fig. 14. Measured and simulated amplitudes of the high-voltage pulse $V(1)$.

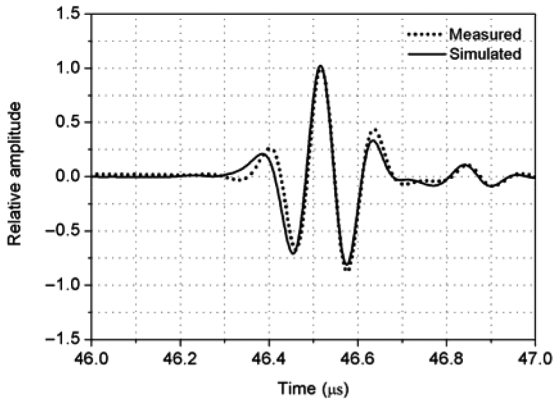

(a)

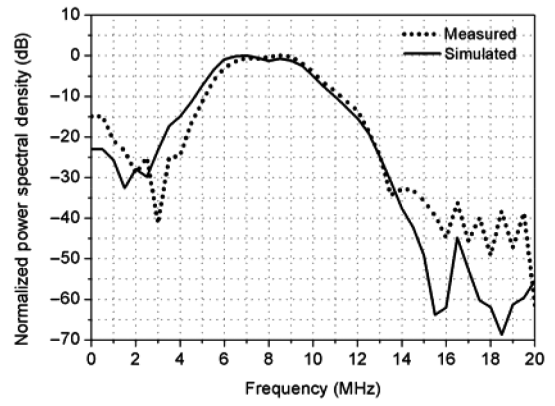

(b)

Fig. 15. Measured and simulated amplitudes of the echo signal $V(2)$ in (a) time domain and (b) frequency domain.

and an acceptable density of input referred noise are both determined by the depth of the target to be imaged; the resolution of the ADC is determined by the required image quality; and also, the bandwidth of the LNA and PGA, the cut-off frequency of the AAF, and the sampling rate of the ADC all depend on the bandwidth of the transducer used in a particular application.

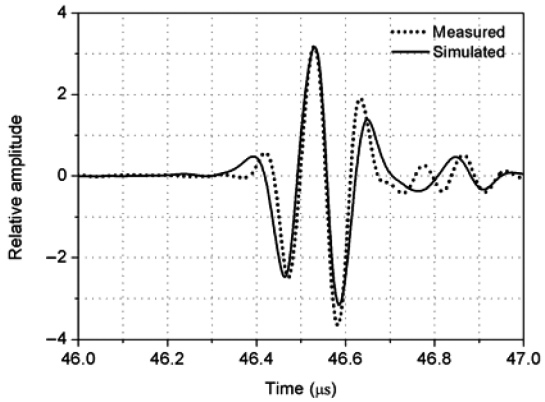

(a)

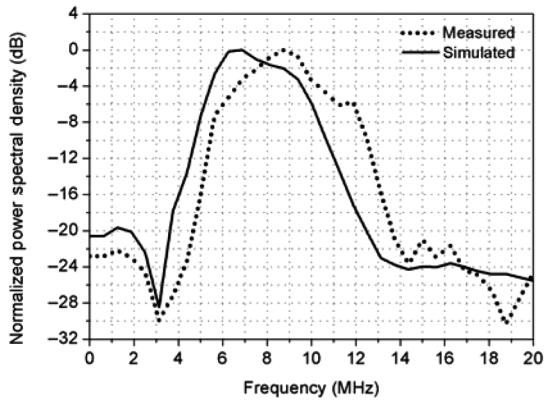

(b)

Fig. 16. Measured and simulated amplitude of the digitized output $V(3)$ in (a) time domain and (b) frequency domain.

V. Conclusion

We have presented a simulator for pulse-echo ultrasound systems, which combines models the high-voltage transmitter, coaxial cable, transducer, ultrasound field, and front-end receiver in a single MATLAB/Simulink simulation. A system designer can generate the high-voltage pulses that they require by configuring the input parameters of the high-voltage transmitter model. The acoustic subsystem model, which consists of the coaxial cable, transducer, and ultrasound field, is based on samples of the transmitted pulse and received echo. From these samples, a transfer function of the acoustic subsystem is formulated in the Laplace s-domain using the MATLAB *rationalfit* function, and is then converted to a Simulink model. To express the voltage division caused by impedances, models of the interfacing electronics one for transmit and one for receive mode, are inserted between subsystems. These models are also based on transfer functions, which are obtained by measuring the impedance of the acoustic subsystem, the high-voltage transmitter, and the front-end receiver. The model of the front-end receiver includes the main nonidealities (i.e., amplifier noise, harmonic distortion, and sampling clock jitter) which have the potential to reduce system performance significantly.

This simulator is intended to facilitate the design of matching networks and system optimization. In particular, the availability of a model of the high-voltage transmitter makes it easier to discover how characteristics of the transmitted pulse, such as its magnitude and frequency, the number of peaks, rise and fall times, and jitter and noise will affect the received echo. Designers can also examine the effects of the front-end receiver parameters on the whole system. We have demonstrated that our simulator is accurate enough to contribute to the development of ultrasound systems by comparing the simulated results with measured data from a commercial ultrasound system.

REFERENCES

[1] B. A. J. Angelsen, H. Torp, S. Holm, K. Kristoffersen, and T. A. Whittingham, "Which transducer array is best?" *Eur. J. Ultrasound*, vol. 2, no. 2, pp. 151–164, 1995.

[2] H. Huang and D. Paramo, "Broadband electrical impedance matching for piezoelectric ultrasound transducers," *IEEE Trans. Ultrason. Ferroelectr. Freq. Control*, vol. 58, no. 12, pp. 2699–2707, Dec. 2011.

[3] E. Brunner, "Ultrasound system considerations and their impact on front-end components," in *Analog Dialogue*. Norwood, MA, USA: Analog Devices Inc., 2002, vol. 36, no. 3.

[4] A. Püttmer, P. Hauptmann, R. Lucklum, O. Krause, and B. Henning, "SPICE model for lossy piezoceramic transducers," *IEEE Trans. Ultrason. Ferroelectr. Freq. Control*, vol. 44, no. 1, pp. 60–66, Jan. 1997.

[5] E. Maione, P. Tortoli, G. Lypacewicz, A. Nowicki, and J. M. Reid, "PSpice modelling of ultrasound transducers: comparison of software models to experiment," *IEEE Trans. Ultrason. Ferroelectr. Freq. Control*, vol. 46, no. 2, pp. 399–406, Mar. 1999.

[6] J. van Deventer, T. Lofqvist, and J. Delsing, "PSpice simulation of ultrasonic systems," *IEEE Trans. Ultrason. Ferroelectr. Freq. Control*, vol. 47, no. 4, pp. 1014–1024, Jul. 2000.

[7] R. Guelaz, D. Kourtiche, and M. Nadi, "Ultrasonic piezoceramic transducer modeling with VHDL-AMS: Application to ultrasound nonlinear parameter simulations," *IEEE Sensors J.*, vol. 6, no. 6, pp. 1652–1661, Dec. 2006.

[8] J. Johansson, P.-E. Martinsson, and J. Delsing, "Simulation of absolute amplitudes of ultrasound signals using equivalent circuits," *IEEE Trans. Ultrason. Ferroelectr. Freq. Control*, vol. 54, no. 10, pp. 1977–1982, Oct. 2007.

[9] N. Aouzale, A. Chitnalah, and H. Jakjoud, "Experimental validation of SPICE modeling diffraction effects in a pulse-echo ultrasonic system," *IEEE Trans. Circuits Syst. II Exp. Briefs*, vol. 56, no. 12, pp. 911–915, Dec. 2009.

[10] W. P. Mason, *Electromechanical Transducers and Wave Filters*. New York, NY, USA: Van Nostrand, 1948.

[11] M. Redwood, "Transient performance of a piezoelectric transducer," *J. Acoust. Soc. Amer.*, vol. 33, no. 4, pp. 527–536, Apr. 1961.

[12] R. Krimholtz, D. A. Leedom, and G. L. Matthaei, "New equivalent circuit for elementary piezoelectric transducers," *Electron. Lett.*, vol. 6, no. 13, pp. 398–399, Jun. 1970.

[13] W. Marshall Leach, Jr., "Controlled-source analogous circuits and SPICE models for piezoelectric transducers," *IEEE Trans. Ultrason. Ferroelectr. Freq. Control*, vol. 41, no. 1, pp. 60–66, Jan. 1994.

[14] L. Capineri, L. Masotti, M. Rinieri, and S. Rocchi, "Ultrasonic transducer as a black-box: Equivalent circuit synthesis and matching network design," *IEEE Trans. Ultrason. Ferroelectr. Freq. Control*, vol. 40, no. 6, pp. 694–703, Nov. 1993.

[15] J. A. Jensen, "Field: A program for simulating ultrasound systems," *Med. Biol. Eng. Comput.*, vol. 34, Suppl. 1, pt. 1, pp. 351–353, 1996.

[16] F. Lindvall. (2013, Jun.) *The DREAM Toolbox* [Online]. Available: http://www.signal.uu.se/Toolbox/dream/

[17] M. E. Frijlink, H. Kaupang, T. Varslot, and S.-E. Masøy, "Abersim: A simulation program for 3D nonlinear acoustic wave propagation for arbitrary pulses and arbitrary transducer geometries," in *Proc. IEEE Ultrason. Symp.*, Nov. 2008, pp. 1282–1285.

[18] S. Holm, "Ultrasim– A toolbox for ultrasound field simulation," in *Proc. Nordic MATLAB Conf.*, Oslo, Norway, Oct. 2001, pp. 1–5.

[19] F. Varray, O. Basset, P. Tortoli, and C. Cachard, "CREANUIS: A nonlinear radio frequency ultrasound image simulator," *Ultrasound Med. Biol.*, vol. 39, no. 10, pp. 1915–1924, 2013.

[20] A. Ebadi, M. Mirzaie, and S. A. Gholamian, "A comparison between electrical circuit and finite element modeling methods for performance analysis of a three-phase induction motor under voltage unbalance," *Iran. J. Electr. Electron. Eng.*, vol. 8, no. 2, pp. 188–194, Jun. 2012.

[21] G. Matrone, A. S. Savoia, M. Terenzi, G. Caliano, F. Quaglia, and G. Magenes, "A volumetric CMUT-based ultrasound imaging system simulator with integrated reception and μ-beamforming electronics models," *IEEE Trans. Ultrason. Ferroelectr. Freq. Control*, vol. 61, no. 5, pp. 792–804, May 2014.

[22] R. Reeder and C. Petersen, "The AD9271—A revolutionary solution for portable ultrasound," in *Analog Dialogue 41–07*. Norwood, MA, USA: Analog Devices Inc., Jul. 2007.

[23] B. Gustavsen and A. Semlyen, "Rational approximation of frequency domain responses by vector fitting," *IEEE Trans. Power Del.*, vol. 14, no. 3, pp. 1052–1061, Jul. 1999.

[24] R. Zeng and J. Sinsky, "Modified rational function modeling technique for high speed circuits," in *Proc. IEEE MTT-S Int. Microw. Symp. Dig.*, San Francisco, CA, USA, Jun. 11–16, 2006, pp. 1951–1954.

[25] Quad ±90 V, ±2A, 3/5 levels, High-speed Ultrasound Pulser, STMicroelectronics, Geneva, 2012, STHV748 DataSheet.

[26] Fully integrated, 8-channel ultrasound analog front end with passive CW mixer, 0.75 nV/rtHz, 14/12-Bit, 65 MSPS, 153 mW/CH, Texas Instruments Inc., Dallas, TX, 2014, AFE5808 DataSheet.

[27] S. Barra, A. Dendouga, S. Kouda, and N. Bouguechal, "Simulink behavioral modeling of a 10-bit pipelined ADC," *J. Circuits Syst. Comput.*, vol. 22, no. 2, pp. 134–142, Feb. 2013.

[28] S. S. Corbett III, "The influence of nonlinear fields on miniature hydrophone calibration using the planar scanning technique," *IEEE Trans. Ultrason. Ferroelectr. Freq. Control*, vol. 35, no. 2, pp. 162–167, Mar. 1988.

[29] L. Svilainis and V. Dumbrava, "Evaluation of the ultrasonic transducer electrical matching performance," *Ultrasound*, vol. 62, pp. 16–21, 2007.

Taehoon Kim received the B.S. and M.S. degrees in electrical engineering from Seoul National University, Seoul, South Korea, in 2009 and 2012, respectively, where he is currently pursuing the Ph.D. degree in electrical and computer engineering.

His research interests include sensor interface circuits, analog front-end circuits, and analog-to-digital converters for ultrasound medical imaging application.

Sangmin Shin received the B.S. degree in electrical engineering and computer science from the University of California at Berkeley, Berkeley, CA, USA, in 2013. He is currently pursuing the Ph.D. degree in electrical and computer engineering from Seoul National University, Seoul, South Korea.

His research interests include analog and mixed-signal integrated circuits and systems.

Hyongmin Lee was born in Seoul, South Korea, in 1984. He received the B.S. and M.S. degrees in electrical engineering from Seoul National University, Seoul, South Korea, in 2008 and 2010, respectively, where he is currently pursuing the Ph.D. degree in electrical and computer engineering.

His research interests include analog and mixed-signal integrated circuits and systems.

Hyunsook Lee received the B.S. degree in electronic engineering from Chosun University, Gwangju, South Korea, in 1999.

From 2000 to 2007, she was a Principal R&D Engineer with Ace Technologies, Incheon, South Korea. She joined Alpinion Medical Systems, Seoul, South Korea, where she is currently a Senior Principal Engineer of R&D Division. Her research interests include general and continuous-wave (CW) analog circuits designing and development of medical ultrasound system.

Heewon Kim received the B.S. degree in mechanical design engineering from Kumoh National Institute of Technology, Gumi, South Korea, in 2001, and the M.S. degree in mechanical engineering from Kyungpook National University, Daegu, South Korea, in 2003.

From 2003 to 2009, he was a Principal R&D Engineer with the Siemens Ultrasound Division, Pohang, South Korea. He joined Alpinion Medical Systems, Seoul, South Korea, where he is currently a Senior Principal Engineer of R&D Division. His research interests include acoustic designing and development of medical ultrasound transducer.

Eunhee Shin received the B.S. degree in electrical design engineering from Daegu University, Daegu, South Korea, in 2008, and the M.S. degree in sensor engineering from Kyungpook National University, Daegu, South Korea, in 2010.

She joined Alpinion Medical Systems, Seoul, South Korea, where she is currently a Senior Engineer of R&D Division. Her research interests include acoustic designing and development of medical ultrasound transducer.

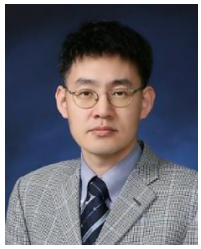

Suhwan Kim (S'97–M'01–SM'07) received the B.S. and M.S. degrees in electrical engineering and computer science from Korea University, Seoul, South Korea, in 1990 and 1992, respectively, and the Ph.D. degree in electrical engineering and computer science from the University of Michigan, Ann Arbor, MI, USA, in 2001.

From 1993 to 1999, he was with LG Electronics, Seoul, South Korea. From 2001 to 2004, he was a Research Staff Member with IBM T. J. Watson Research Center, Yorktown Heights, NY, USA. In 2004, he joined Seoul National University, Seoul, South Korea, where he is currently a Professor of Electrical Engineering. His research interests include high-performance and low-power analog and mixed-signal integrated circuits, high-speed I/O circuits, and power electronics.

Dr. Kim served as a Guest Editor for the *IEEE Journal of Solid-State Circuits* special issue on the IEEE Asian Solid-State Circuits Conference. He has also served as the General Cochair and Technical Program Chair for the IEEE International System-on-Chip (SoC) Conference. He has participated multiple times on the Technical Program Committee of the IEEE International SOC Conference, the International Symposium on Low-Power Electronics and Design, the IEEE Asian Solid-State Circuits Conference, and the IEEE International Solid-State Circuits Conference. He received the 1991 Best Student Paper Award from the IEEE Korea Section and the First Prize (Operational Category) in the VLSI Design Contest of the 2001 ACM/IEEE Design Automation Conference.